Contract No:

This document was prepared in conjunction with work accomplished under Contract No. 89303321CEM000080 with the U.S. Department of Energy (DOE) Office of Environmental Management (EM).

Disclaimer:

Time Domain Thermoreflectance (TDTR) Studies of Microstructural Characterization of as-Fabricated and/or Irradiated TPBAR Components

Eliel Villa-Aleman

September 2021

SRNL-STI-2021-00419, Revision 0

DISCLAIMER

Printed in the United States of America

Prepared for
U.S. Department of Energy

SRNL-STI-2021-00419
Revision 0

Keywords: Tritium Science Research
Retention: *Varies*

Time Domain Thermoreflectance (TDTR) Studies of Microstructural Characterization of as-Fabricated and/or Irradiated TPBAR Components

Eliel Villa-Aleman

September 2021

Savannah River National Laboratory is operated by Battelle Savannah River Alliance for the U.S. Department of Energy under Contract No. 89303321CEM000080.

REVIEWS AND APPROVALS

AUTHORS:

_____

Eliel Villa-Aleman, Global Security and Safeguards Date

APPROVAL:

_____

Charles R. Shick, Manager Date
Trace Nuclear Measurement Technology

EXECUTIVE SUMMARY

Paddock et al. demonstrated for the first-time the measurement of thermal diffusivity from thin metal films using picosecond transient thermoreflectance in 1986. This project attempted to use a similar experimental setup based on a femtosecond time domain thermoreflectance (TDTR) to measure the damage to the crystal lattice of $LiAlO_2$ from irradiation in the reactor and production of tritium and helium. The TDTR is based on a pump-probe laser configuration where the pump laser is used to heat the sample and the probe laser is used to follow the thermal evolution created by the pump laser. The goal for this project is to measure the differences in thermal diffusivity between $LiAlO_2$ and the irradiated $LiAlO_2$ sample in a reactor. Unfortunately, COVID-19 restricted laboratory research time and the availability of researchers capable to conduct TDTR work. In addition, the ultrafast laser (Astrella 35fs laser) required to conduct the work was inoperable making this particulate work impossible to conduct in FY20 and FY21.

The purpose of the thermal diffusion measurements with a TDTR setup is to probe the damage and disorder to the crystal lattice of pristine and irradiated samples. Since TDTR was not available for this work, a different approach using Raman and luminescence spectroscopy was used to characterize the crystal lattice damage in $LiAlO_2$ from irradiation.

The Raman and luminescence spectroscopy of un-irradiated and irradiated $LiAlO_2$ pellets were studied for the first time with numerous excitation wavelengths (457, 488, 514, 633, and 785 nm). Although the Raman spectrum of $LiAlO_2$ was previously published by Hu et al., our high-resolution Raman spectra provided a method to use the full-width half maximum (FWHM) of the Raman bands to identify damage in the $LiAlO_2$ crystal lattice due to irradiation of the sample in a reactor. Additional bands were also observed in our Raman spectra not previously published. In contrast to the small spectral region monitored in early research (1000 cm^{-1}), SRNL research explored the presence of additional bands up to 4000 cm^{-1}.

Raman spectra from the surface and bulk material identified small differences in spectral features. Raman bands measured at the surface were primarily identified as hydrocarbons impurities (peaks in the 2900 cm^{-1} region, most likely from contamination impurities) and free OH bonding (sharp band in the 3400 - 3700 cm^{-1} spectral region) most likely from water molecules chemically bonded to the oxygen of the $LiAlO_2$. Bands were clearly identified at 2857, 2934, 3444, 3498, 3545, and 3656 cm^{-1}.

Strong luminescence bands were observed at ~713.3 nm, although at least four other bands were observed in the luminescence spectrum with the 514 nm excitation wavelength. Significant luminescence was observed with the 633 nm excitation wavelength where additional bands became clearly observable.

The irradiation of $LiAlO_2$ resulted in a sample with high luminescence in the visible spectrum. The Raman spectrum of $LiAlO_2$ acquired with the 785 nm showed significant damage to the crystal lattice through the FWHM of the bands. The broadening (FWHM) of the bands is indicative of damage to the material upon irradiation. The luminescence of $LiAlO_2$ also significantly changed upon irradiation. New bands were observed in the material. The data shows that Raman and luminescence spectroscopy can be used to probe the damage to the material even though most tritium and helium were removed from the $LiAlO_2$ sample by heating in a furnace.

TABLE OF CONTENTS

LIST OF TABLES

LIST OF FIGURES

LIST OF ABBREVIATIONS

SRNL	Savannah River National Laboratory
TDTR	Time Domain Thermoreflectance
FWHM	Full-Width Half-Maximum

1.0 Introduction

Paddock et al. in 1986 demonstrated for the first-time the measurement of thermal diffusivity from thin metal films using picosecond transient thermoreflectance[1]. The setup is based on a pump-probe laser configuration where the ultrafast pump laser is used to heat the material surface and induce a change in the index of refraction of the material, and thus a change in the optical properties while the probe laser is used to follow the temporal evolution of the optical properties. The TDTR technology evolved from a picosecond laser to a femtosecond laser. Different colors for the pump and probe beams and the optical modulation of laser beam were used to provide better discrimination and an enhanced signal to noise ratio. These improvements resulted in the understanding of thermal properties of nanoparticles with dimensions less than 10 nm. This pump-probe technique can be used to demonstrate the detection and damage quantification of He bubbles in metals and ceramics, such as $LiAlO_2$. The formation of ^3He bubbles from tritium beta decay results in damage to the crystal lattice producing phonon scattering points. The lifetime of the phonons produced during the laser heating pulse is shortened by defects in the crystal lattice. This effect is valuable to determine the crystal lattice damage from beta decay and precipitation of He bubbles. Figure 1 shows the design of the TDTR setup at SRNL. Figure 2 shows the current development of the TDTR setup at SRNL. Figure 3 shows the pump-probe approach of the TDTR.

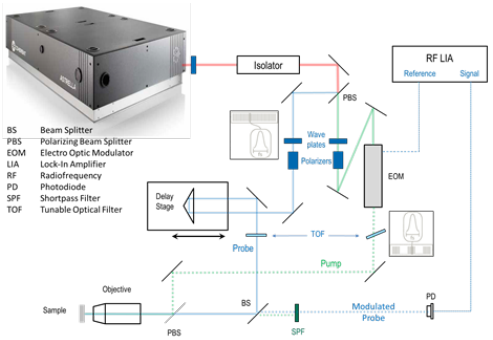

Figure 1. Design of the TDTR setup at SRNL.

Figure 2. Current development of the TDTR setup at SRNL.

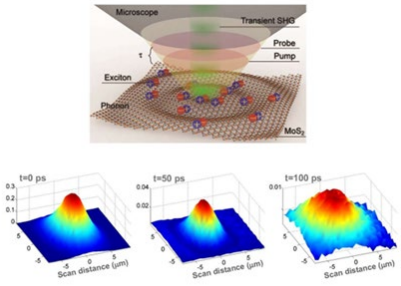

Figure 3. Pump-probe approach of the TDTR.

The crystal lattice damage due to tritium decay correlates to the alpha decay and crystal lattice damage in the PuO_2 system. We recently published the application of Raman spectroscopy in the characterization of alpha decay damage to the crystal lattice [2]. Similarly, Weisensee et al. [3] measured the effect of ion irradiation on the thermal conductivity of UO_2 and U_3O_8 using TDTR. Cheaito et al. [4] used TDTR to measure thermal conductivity of radiation-induced damage of ZIRLO (a low oxidation Zircaloy), and in silicon. Cheaito et al. identified the influence of lattice impurities to the thermal conductivity of materials. For instance, oxygen impurities changed thermal conductivity of beta-Si_3N_4 from 120 W/m-K to 88W/m-K. SRNL TDTR setup was funded in an LDRD project to measure the effect of He bubbles in steel samples. TDTR is the key technology for the characterization of materials and components exposed to radiation based on thermal conductivity measurements.

The thermal properties of $LiAlO_2$, the material responsible for producing tritium in a reactor, can be characterized using TDTR. The TDTR technique offers the opportunity to understand how reactor exposure can affect the material and how it dissipates the heat. It is expected that TDTR might differentiate inner and outer rods and the location within a bundle based on the exposed temperature/radiation and damage to the material. The technique is also expected to provide a vibrational spectrum by taking the Fourier transform of the oscillations in the decay curve. It is expected that TDTR will be able to monitor the lattice damage at different depths within the pellet (wavelength dependent penetration). The proposed study will help provide information on the mechanisms controlling the integrity and tritium loss within the $LiAlO_2$ pellets.

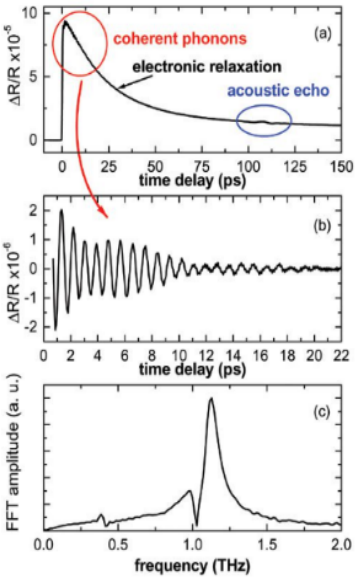

Figure 4. (a) Time-resolved reflectivity change of a Si/Mo extreme UV mirror. (b) Extracted coherent phonon oscillations in the first 20ps. Note that the amplitude of the coherent oscillations are minute changes of the reflectivity only. (c) Numerical Fourier transform of the data in (b). Fast Fourier transform.

The proposed work has three main tasks: The first task is to characterize the TDTR of unirradiated $LiAlO_2$ and determine the Raman spectrum, thermal diffusion and heat capacitance of the material. A pulsed laser beam will be used to induce crystal lattice damage and provide a methodology to induce damage to the $LiAlO_2$ and relate to irradiation damage. Temperature decomposition/annealing of $LiAlO_2$ material will be studied using laser-induced heating in the same way it was used to study the crystal lattice damage of PuO_2 particulate aggregates calcined at 450, 650 and 1100˚C.

The second task will irradiate $LiAlO_2$ with a neutron beam, explore the effect of the neutron beam and then bring the sample into a clean laboratory for analysis with advanced vibrational spectroscopic tools. Cells were developed to bring uranium with tritium for analysis in our clean laboratory. This phase will explore handling of radioactive material, extraction of particulates from pellets, tritium exposure and encapsulation, to conduct analyses in a clean laboratory. Irradiation of enriched (Li-6) $LiAlO_2$ with a neutron generator might be used to study damage to the material. The third task of the project is to document the work and write a report describing the methodologies.

2.0 Experimental Procedure

The proposed research attempted to investigate the thermal and spectroscopic properties of un-irradiated and reactor irradiated $LiAlO_2$. This research was conducted with $LiAlO_2$ samples acquired from the Pacific Northwest Laboratory (PNNL). Several un-irradiated $LiAlO_2$ samples were used in this study (ELAM-017, ELAM-20, and ELAM-22). The samples provided by PNNL are white cylinders approximately 2” long. One example of the $LiAlO_2$ samples is shown in Figure 5.

Figure 5. $LiAlO_2$ samples used in the experimental characterization with Raman and luminescence spectroscopy.

In contrast to the simplicity of the experimental setup used in the study of un-irradiated samples, the irradiated samples, even though they have been heated to extract tritium from the material, contain significant amount of tritium. ^{6}Li in the $LiAlO_2$ absorbs neutrons in a reactor to produce ^{3}H according to the equation: $\mathbf{{}^{6}_{3}Li + n \rightarrow {}^{4}_{2}He + {}^{3}_{1}T}$. ^{3}H decays to insoluble ^{3}He by beta decay. The production of ^{3}He clusters cause swelling and deformation of the material. Reactor irradiation and tritium decay to helium induces defects in the crystal lattice of the $LiAlO_2$ material. Thermal diffusivity, heat capacity, Raman and luminescence spectroscopy are useful tools to evaluate changes in the crystal lattice induced by the irradiation.

1) Plate Nuts
2) Cell Window
3) Cell Base
4) Carbon Tape
5) Bolts
6) Copper Gaskets
7) Spare Short Cell Base (only use if necessary)
8) Spare Bolts and Plate Nuts

Figure 6. Double containment cell used in the clean laboratory for spectroscopic analysis.

The tritium content in the sample precluded any direct measurements with the sample in an open environment and therefore, a sealed ConFlat cell is required for these measurements. Since our laboratory is a clean laboratory and the building conducts low-level tritium measurements, tritium quantities are kept low in the building. The amount of material with tritium inside of the cell was kept under 1 Ci. PNNL provided an irradiated sample of about 0.5 x 0.5 cm^2 attached to a sticky tape inside of a cell with a quartz window for optical measurements. Figure 6 shows the kit SRNL sent to PNNL to contain the irradiated $LiAlO_2$ sample. Figure 7 shows the ConFlat cell with the small piece of $LiAlO_2$ in the cell.

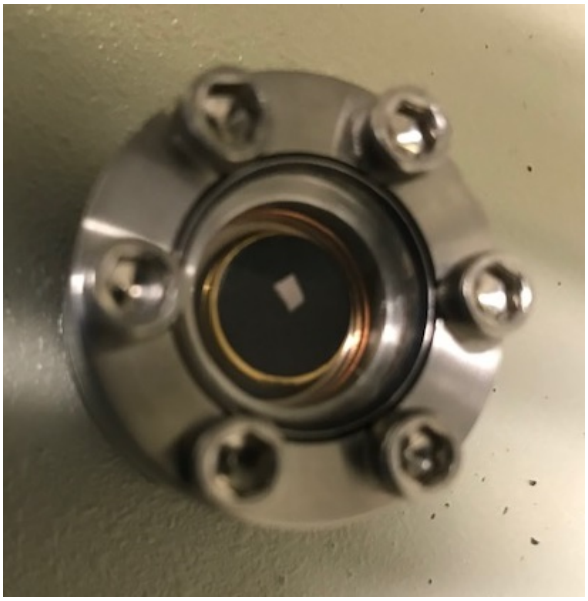

Figure 7. ConFlat cell with a small piece of irradiated $LiAlO_2$.

COVID-19 significantly affected the direction of this project. Limited personnel in the laboratory and personal health issues precluded the scientists primarily working in this area from conducting research. In addition, to COVID-19, the 35fs Astrella laser used in the TDTR was inoperable and could not be used in the TDTR work. An alternate plan to address these two issues resulted in the utilization of Raman spectroscopy for the characterization of $LiAlO_2$ and the irradiated sample.

3.0 Results and Discussion

Raman microspectroscopy is a useful technique to infer the degree of crystalline order in materials and the effect of irradiation in the material. Irradiation of a material results in crystal lattice damage. Figure 8 shows crystal lattice damage during radiation. Damage to the crystal lattice is responsible for changes in the full-width half maximum (FWHM) of the bands and the growth of new vibrational bands due to the relaxation of the spectroscopic selection rules. Previous work funded by the Defense Nuclear Nonproliferation Research and Development (DNN R&D) NA22 Nuclear Forensics Program in 2015 was dedicated to understanding signatures in the Raman spectrum of PuO_2 related to aging. Double-walled containment cells were developed to transfer milligram quantities of PuO_2 samples from a radiological hood to a clean laboratory for spectroscopic analysis using Raman and infrared spectroscopy. Micro-Raman spectra were acquired with a modified commercial system (LabRAM HR800 UV, Horiba Jobin-Yvon). Details of the Raman microspectroscopy system were described previously [2]. The alpha decay effect on the Raman spectrum of PuO_2 – 240 calcined at 1000˚C was followed over 16 months. Figures 9 and 10 shows the temporal Raman spectra of the PuO_2 T_{2g} band due to auto-irradiation. The damage to the crystal was established with the relationship:

$$\frac{\Delta a}{a_0} = A(1 - e^{-B\tau t})$$

where a_0 is the lattice parameter after preparation, Δa is the change in lattice parameter via self-radiation, A and B are constants, τ is the decay constant of actinide isotope and t is storage time. This ongoing work provided unique information of a radiological material from areas as small as 5 microns in dimensions. Clearly, if band properties in the Raman spectrum can be used to follow the auto-irradiation in the PuO_2 system, a similar approach can be used to study the irradiation of $LiAlO_2$ and tritium formation via damage to the crystal lattice.

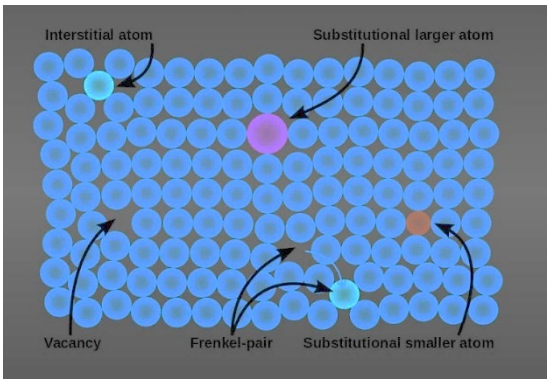

Figure 8. Defects in a crystal latticed from irradiation of the material. Typical defects include interstitial atoms, vacancies, and Frenkel pairs.

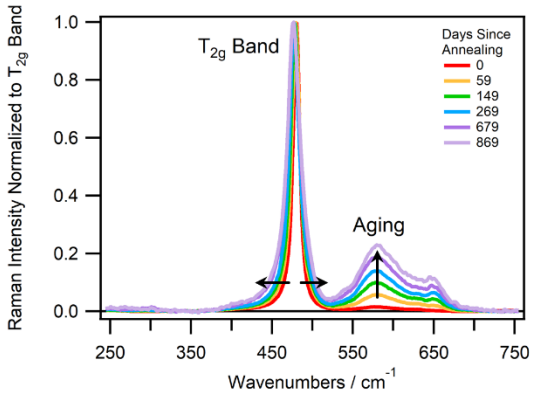

Figure 9. Raman spectra of the T_{2g} band. The alpha decay damage in the crystal is responsible for the changes in the FWHM and the new bands.

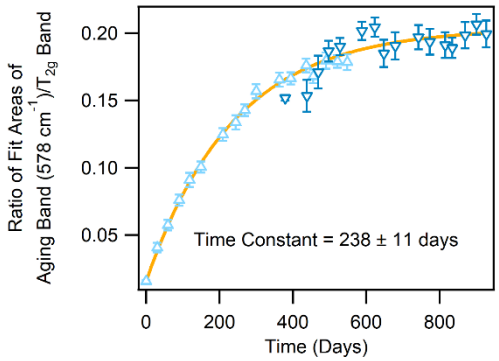

Figure 10: Relative changes in Raman spectral features as a function of time. Ratio of aging band to T_{2g} areas have similar decay curve to the $\frac{\Delta a}{a_0}$ measured by XRD.

Since Raman spectroscopy can provide the degree of crystal lattice damage, it was decided to investigate the differences between un-irradiated and irradiated damage $LiAlO_2$. The Raman spectrum of $LiAlO_2$ was compared with the published Raman spectrum in the literature. The Raman spectrum acquired with our microscope setup shows much higher resolution than the Raman spectrum published by Hu et al. Besides Raman spectrum, the luminescence spectrum showed differences between the unirradiated and irradiated material. The 633 and 514 nm excitation laser wavelengths of the un-irradiated material shows a strong luminescence around 713.3 nm related most likely to Cr impurities where Al atoms are replaced in the crystal lattice with Cr. Meanwhile, the irradiated material was observed to luminescence significantly across the visible spectral region indicating a variety of new defects in the crystal not present in the unirradiated material.

The Raman spectrum of $LiAlO_2$ has been measured in the literature [4]. Several Li-O vibrational bands were identified in the ~200 – 400 cm^{-1} spectral region. Just like in the case of PuO_2 self-irradiation, irradiation of $LiAlO_2$ in a reactor is expected to produce significant lattice damage to the crystal during the tritium and helium formation. The positions of the Li and Al atoms in the crystal can be significantly affected during irradiation, therefore changing the expected Raman spectrum. The radiation flux and the generation of tritium gas, tritium oxide and He bubbles will determine the extent of the lattice damage to the $LiAlO_2$ material. Frenkel ion pairs in the crystal can significantly change the spectrum. This work might provide new leads to developing understanding of mechanisms controlling the integrity and tritium loss within the $LiAlO_2$ pellets.

Figure 11 shows the Raman spectrum of $LiAlO_2$ recorded by Q. Hu et al. with a 532 nm laser. Table 1 shows the Raman band assignments observed in the spectrum. The intense $B_2^{(1)}$ band located at 124 cm^{-1} is related to a vibrational mode between LiO_4-AlO_4 group. Low frequencies in the 187 – 398 cm^{-1} spectral range correspond to bending and stretching modes of the Li-O moeity and stretching modes of the Li-O-Al moeity. Vibrational modes in the 508 to the 844 cm^{-1} spectral region are identified as bending and stretching mode for the Al-O bond.

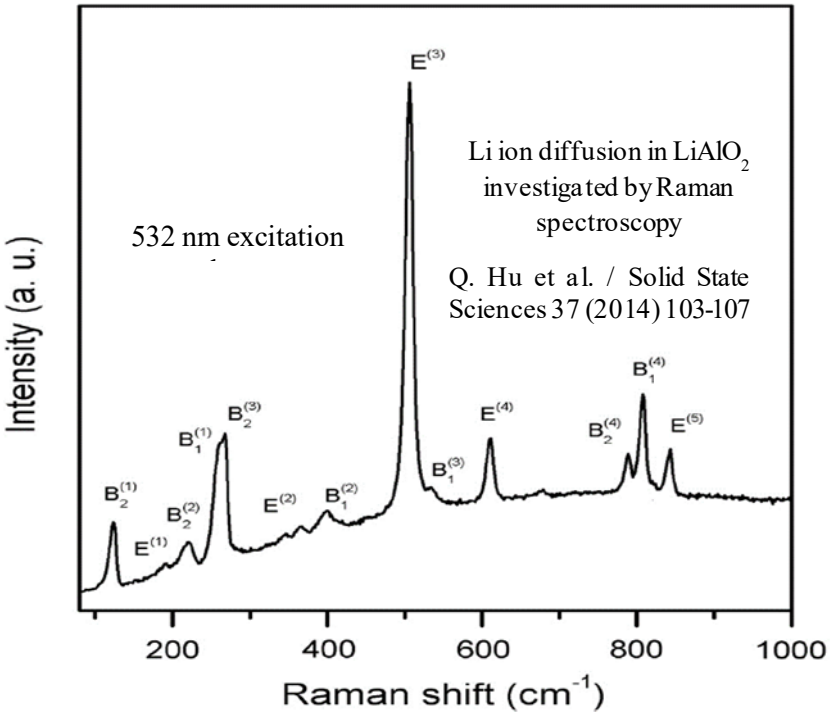

Figure 11. Raman spectrum of $LiAlO_2$ recorded by Hu et al.

The Raman spectrum of $LiAlO_2$ shown in Figure 12 was acquired with higher resolution than the one published by Hu et al. in Figure 11. The higher resolution of our experimental setup is clearly shown in the two bands located at 262.3 and 269.5 cm^{-1}. The Raman spectrum with the 514 nm is devoid of luminescence in contrast to the large background observed in the Hu et al. spectrum. Additional Raman bands were also present at 159.3, 347.5, 541.9, 677.3, and 1057.3 cm^{-1}. The 159.3 and 1057.3 cm^{-1} were very broad suggesting significant disorder of the bonds. Other bands in the spectrum are also

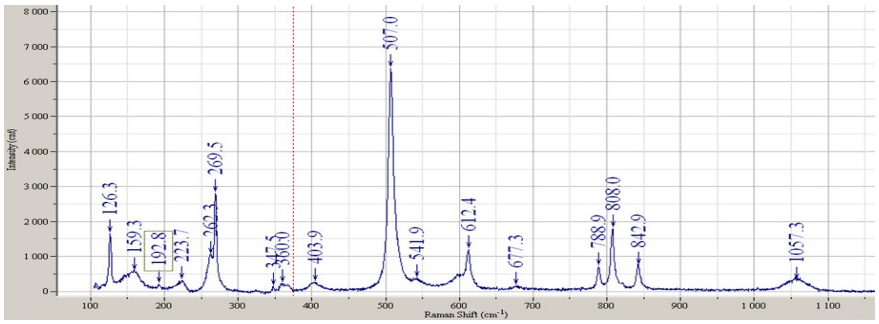

broad suggesting multiple bands or different types of bonding to different chemical structures. Lifetime of the phonon mode can also affect the FWHM of the band. Table 2 shows the bands recorded by SRNL.

Figure 12. Raman spectrum of $LiAlO_2$ acquired with a 488 nm excitation laser.

Table 1. Raman bands of gamma-$LiAlO_2$, tentative assignments, ω_{exp}, ω_{cal} from Hu et al. published work and ω_{exp} from Villa-Aleman (this work) in cm^{-1} units.

Raman mode	**Mode description**	**ω_{exp} Hu et al.**	**ω_{cal} Hu et al.**	**ω_{exp} Villa-Aleman**
$B_2^{(1)}$	LiO_4-AlO_4	124	117	126.3
				159.3
$E^{(1)}$	Li-O-Al bending	187	185	192.8
$B_2^{(2)}$	Li-O stretching	220	230	223.7
$B_1^{(1)}$	Li-O-Al stretching	260	270	262.3
$B_2^{(3)}$	Li-O-Al stretching	268	278	269.5
				347.5
$E^{(2)}$	Li-O bending	366	382	360.0
$B_1^{(2)}$	Li-O stretching	398	388	403.9
$E^{(3)}$	Al-O bending	508	494	507.0
$B_1^{(3)}$	Al-O stretching	540	530	541.9
$E^{(4)}$	Al-O bending	613	625	612.4
				677.3
$B_2^{(4)}$	Al-O stretching	791	737	788.9
$B_1^{(4)}$	Al-O stretching	809	793	808.0
$E^{(5)}$	Al-O bending	844	799	842.9
				1057.3
	C-H stretch			2857
	C-H stretch			2934
	O-H stretch			3444
	O-H stretch			3498
	O-H stretch			3545
	O-H stretch			3656

Additional research shows that there are spectral differences between the surface and bulk material Raman spectra. The confocal hole in the Raman microscope helped identify the spectral differences.

Figure 13 shows the Raman spectrum with the laser focused above and below the surface of the sample. The upper Raman spectrum in the figure was recorded with laser focused above the sample surface. The middle spectrum acquired with laser focused below the surface of the sample. The bottom Raman spectrum was the result from subtracting spectrum 2 from spectrum 1. Clearly, most the signal in the spectrum is significantly different. Bands located at 2900 cm^{-1} suggest hydrocarbons contamination on the surface. The bands located in the 3400 – 3700 cm^{-1} spectral region are most likely to hydrogen

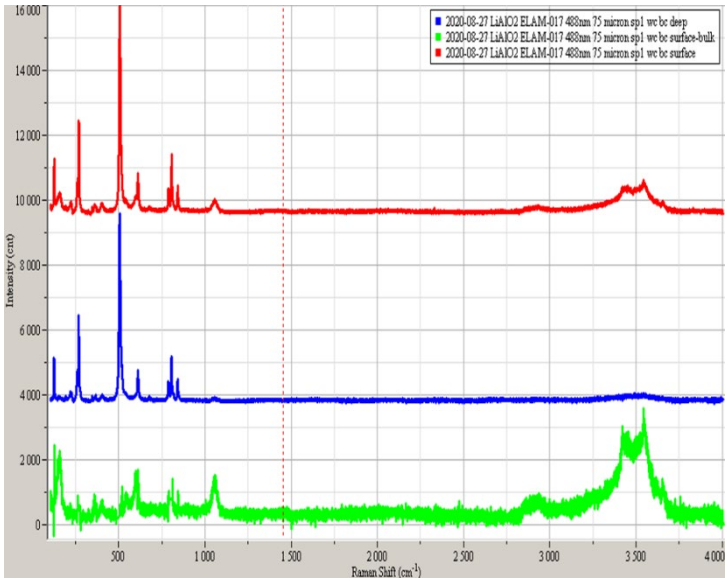

Figure 13. Raman spectra of $LiAlO_2$ from surface and bulk material.

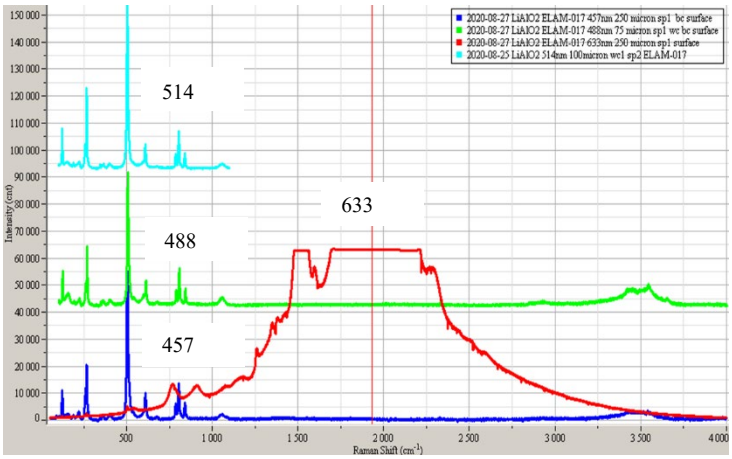

Figure 14. Raman spectra of $LiAlO_2$ with 457, 488, 514, and 633 nm excitation lasers.

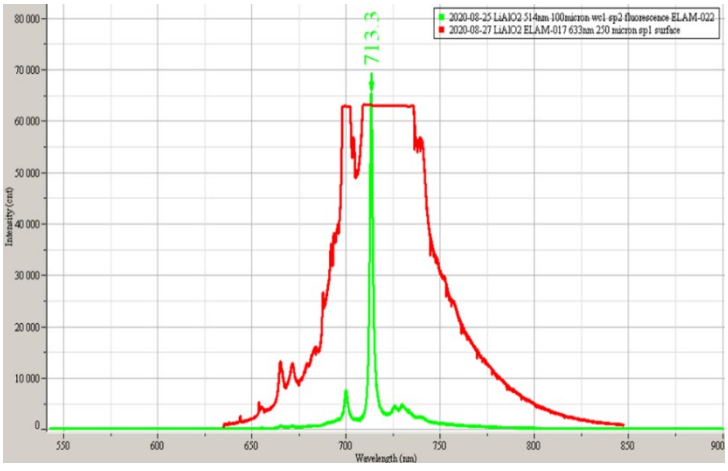

Figure 15. Luminescence spectra of $LiAlO_2$ with a 633 nm and 514 nm excitation lasers.

bonding. The sharpness of the bands suggests free OH on the surface, most likely water attaching to the oxygen of the $LiAlO_2$. Strong broad bands were observed at 159, 1057.3, and a hump in the low side of the 612 cm^{-1} band.

The wavelength dependent Raman spectra of $LiAlO_2$ were studied with four different excitation lasers (457, 488, 514, and 633 nm). Figure 14 shows the Raman spectra acquired at these wavelengths. The 457, 488, and the 514 nm excitation lasers provided similar Raman spectra. The 633 nm laser resulted in a significant luminescence emission with maximum intensity around 713.3 nm as shown in Figure 15. The excitation lasers at 457 and 488 nm cover the 100 – 4000 cm-1 spectral region. Vibrational bands at ~2900 and 3500 cm^{-1} spectral region are indicative of hydrocarbons and OH.

Figure 15 shows the luminescence band acquired with the 633 and the 514 nm excitation lasers. Several luminescence peaks can be observed with the 514 nm excitation laser with the most prominent one located at 713 nm. The luminescence spectrum acquired with the 633 nm laser overwhelms the detector capacity set for Raman spectroscopy measurements. Additional bands can be easily observed with the 633 nm excitation laser.

Significant changes were observed in the Raman and luminescence spectra of irradiated $LiAlO_2$ samples. Figure 16 shows the Raman spectra of unirradiated and irradiated $LiAlO_2$ samples. The significant amount of luminescence in the samples decreased the S/N ratio resulting in noisy Raman spectra from irradiated material. The Raman spectra of the samples were acquired with the 785 nm laser to reduce the luminescence

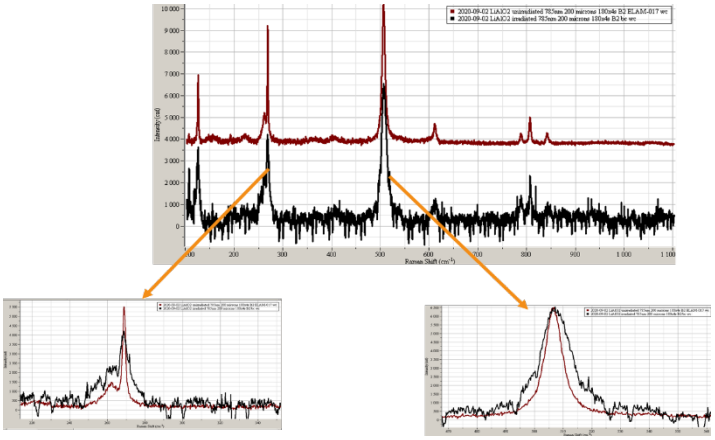

Figure 16. Raman spectra of un-irradiated and irradiated $LiAlO_2$ acquired with a 785 nm laser.

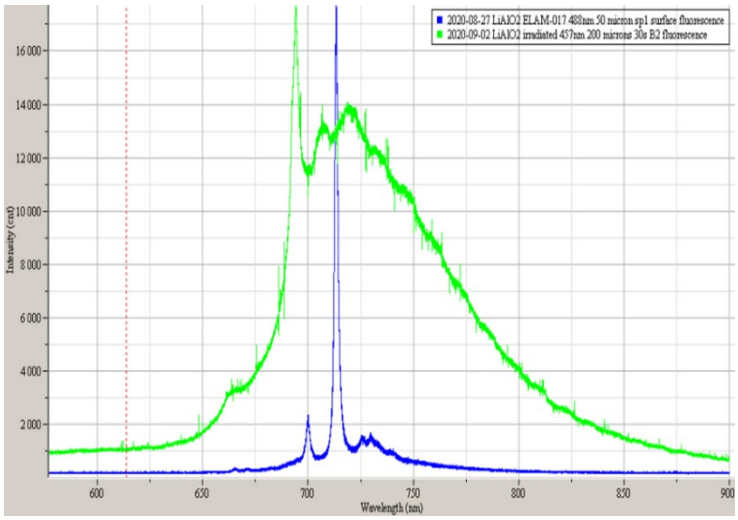

Figure 17. Different luminescent centers observed for the unirradiated and irradiated LiAlO2 samples.

influence in the spectra. The 270 and 507 cm^{-1} bands are shown in Figure 16 where the FWHM of the Raman bands almost doubled in width after irradiation. The FWHM is indicative of damage to the crystal lattice as shown in the PuO_2 spectra after alpha-induced radiation.

Different fluorescent centers were also observed from the irradiated sample. Figure 17 shows a comparison between the luminescence of unirradiated $LiAlO_2$ excited with the 488 nm laser and the luminescence of the irradiated material obtained with the 457 nm laser.

4. Conclusion

Raman and luminescence spectroscopy of $LiAlO_2$ and irradiated $LiAlO_2$ was conducted in this research work. Raman spectra of $LiAlO_2$ at different wavelengths shows similar features. Additional Raman bands were observed in the spectra. Many of the bands are correlated with the surface of the material. A strong luminescence was observed at ~713.3 nm, most likely related to Cr impurities in the material. During irradiation, the crystal lattice was affected significantly based on changes in the Raman spectrum the observation of luminescence centers. Even tritium was removed from the $LiAlO_2$ material at high temperatures, the damage to the crystal lattice is still present. The spectroscopic data acquired from this research suggest that Raman spectroscopy and luminescence spectroscopy could be used to characterize irradiation dose at the material and possibly the type of irradiation on the material.

5. Recommendations, Path Forward or Future Work

Further research using Raman and luminescence spectroscopy, in conjunction with luminescence lifetime is suggested for samples at different locations exposed to different doses of irradiation. This research suggests that it might be possible to separate the effects of tritium and helium bubbles from gamma irradiation to the crystal lattice.

6. References

1. C.A. Paddock and G.L. Eesley, “Transient thermoreflectance from thin metal films”, J. Appl. Phys., 60 (1), 1986, 285-290.
2. E. Villa-Aleman, A.L. Houk, N.J.Bridges, and T.C. Shehee “Raman Spectroscopy: A Tool to Investigate Alpha Decay Damage in a PuO2 Lattice Crystal and Determining Sample Age Since Calcination”, J. Raman Spectrosc., 50(6), 2018, 899-901.
3. P.B. Weisensee, J.P. Feser, and D.G. Cahill, “Effect of ion irradiation on the thermal conductivity of UO_2 and U_3O_8 epitaxial layers”, J. Nucl. Mater., 443, 2013, 212-217.
4.R. Cheaito, C.S. Gorham, A. Misra, K. Hattar, and P.E. Hopkins, “Thermal conductivity measurements via time-domain thermoreflectance for the characterization of radiation induced damage”, J. Mater. Res., 30(09), 2015, 1403-14